Article:
Okeke, G, Hammond, RB and Antony, SJ (2016) Effects of heat treatment on the atomic structure and surface energy of rutile and anatase TiO2 nanoparticles under vacuum and water environments. Chemical Engineering Science, 146. pp. 144-158. ISSN: 0009-2509

https://doi.org/10.1016/j.ces.2016.02.035

In: Chemical Engineerign Science

Effects of heat treatment on the atomic structure and surface energy of rutile and anatase TiO_2 nanoparticles under vacuum and water environments

*George Okeke, Robert B. Hammond, S. Joseph Antony**

School of Chemical and Process Engineering, University of Leeds, Leeds LS2 9JT, UK

*Corresponding author: S.J.Antony@leeds.ac.uk

Abstract

Nanomaterials have become a widely used group of materials in many chemical engineering applications owing to their ability to provide an enhanced level of functional properties compared to their crystalline and bulk counterparts. Here we report fundamental level advancements on how the anatase and rutile phase of TiO_2 nanoparticles chemo-thermally respond between room temperature and the melting temperature under both vacuum and water environments. The current study is based on using molecular dynamics (MD) simulations. We present results on the equilibrium crystal morphology of these phases, structural and surface energy of TiO_2 nanoparticles in the size range of 2-6 nm under different temperatures. Thermodynamic and structural properties, in the form of potential energy and Radial Distribution Functions (RDF's) respectively, are calculated for both forms of TiO_2 nanoparticles. The temperature associated with the melting transition increased with an increase in the particle size in both the phases. The potential energy change associated with the melting transition for anatase was seen to be less than that for rutile nanoparticles. Also the temperature at which the RDF's began to stretch and broaden was observed to be lower for

the case of anatase than rutile, suggesting that rutile attains the most thermal stable phase for the nano particle sizes considered in this study. Structural changes in anatase and rutile nanoparticles under different temperatures revealed that non-spherical (rod-like) rutile nanoparticles tend to be thermodynamically more stable. Surface energy influences the shape of TiO_2 nanoparticles at different temperatures. The increase in the surface energy of nanoparticles under vacuum when compared with that of water environment is higher for the anatase phase than the rutile phase of nanoparticle sizes studied here. The fundamental level simulation results reported here provide a strong platform for potentially accounting for the effects of atomic-scale phase characteristics of TiO_2 nanoparticles and surface energy under different temperature fields in nano processing applications and related multi-scale modelling approaches in future.

Keywords: MD simulations, RDF, surface energy, potential energy, anatase, rutile, titania

1 Introduction

There is growing interest in understanding the material properties of nano-particles, and their link to the performance of nano-particulate dispersions, via modelling over multiple length and time scales. Nano-particles are employed in a number of important engineering applications for example nanofluids for enhanced thermal conductivity. Nanofluids containing titanium dioxide (TiO_2) nanoparticles have been investigated in terms of the particle-scale properties (Okeke et al., 2011; Okeke et al., 2013a). Metal oxide and ceramic particles at the nanometer size can be used in a variety of application areas such as chemical sensors (Zheng et al., 2000), electronics, microporous membranes (Kermanpur et al., 2008), photocatalysis (Onozuka et al., 2006) and catalysis (Soo-Jin Park, 2010; Hu et al., 2002; Xia et al., 2003; Chaudhari et al., 2006; Chen and Weng, 2005; Haverkamp, 2010; Park et al., 2010). Ceramic particles at nanometer sizes have a large surface area per unit mass which may, potentially, enhance

physical, chemical and electrical properties compared to the corresponding properties in the bulk state.

The uses of titania in nanotechnology have been investigated widely as it possesses many desirable properties such as low cost, recyclability, and ease of production in nanostructural forms in comparison with other catalysts (A. Ahmad, 2006). It is also stable in aqueous media (i.e. in both acidic and alkaline solutions). Synthesis of titania nanoparticles can be achieved using methods such as the chloride process (Kirk et al., 1998), sulphate process (Kirk et al., 1998), impregnation (Lihitkar et al., 2007), coprecipitation (Sheng et al., 2012), hydrothermal method (Oh et al., 2006), metal organic chemical vapour deposition methods (Pradhan et al., 2003), and direct oxidation of $TiCl_4$ (A. Ahmad, 2006; Yang et al., 2001).

Titania exists in three crystalline forms namely rutile, anatase and brookite. The most important crystalline forms of titania are rutile and anatase. Understanding the factors that influence the phase stability, for example as a function of particle size, could offer new insights into how microstructures, relative phase composition and properties of titania-based materials can be controlled (Zhang and Banfield, 2000). In bulk form, the rutile phase has been found to be the most stable phase at room temperature (Filyukov et al., 2007), while both anatase and brookite crystalline are known to be metastable, transforming irreversibly to rutile at high temperatures (Okeke et al., 2013b). However, phase stability could differ for titania in the crystalline and at nano particle scale (Koparde and Cummings, 2008). The thermodynamic stability observed in nanocrocrystalline rutile and anatase is dependent on the particle-size. As the size decreases, anatase could attain more stable shape than rutile (Zhang and F. Banfield, 1998) at room temperature and hence the structural characteristics of particles at small scales is important to understand using advanced simulations. This may be the reason why anatase is usually synthesized at ultrafine particle-sizes (Naicker et al., 2005). However, thermal stability characteristics such as melting transition temperature of titania is not yet well studied as a

function of phase especially using MD simulations, an aspect addressed in the present work. Research has shown that a synergy between the two important phases (i.e. anatase and rutile) can greatly influence certain properties of titania such as its photocatalytic properties as the two phases possess different physical properties at nanoscale (Filyukov et al., 2007). Controlling these crystal phases and their morphology is necessary to make them best suited for the desired application. Furthermore, surface properties of nanoparticles including surface energy are known to play an important role in influencing the interaction of particles and the mechanisms that underpin, for example, particle aggregation influences thermal enhancements in nanofluids (Okeke et al., 2011). Such information is not yet well known for different phases of tiania as a function of temperature. This aspect is also addressed in the present work.

Molecular dynamics (MD) simulation (Cai et al., 2008) is used in this study to investigate thermo-physical properties of anatase and rutile TiO_2 nanoparticles. Simulations were performed for initially spherical particles with diameter ranging from 2 to 6 nm and for different temperatures in the range from 300 to 3000 K. Thermodynamic and structural properties, including radial distribution functions and surface energy for anatase and rutile polymorphs are reported for different particle sizes as a function of temperature.

This paper is organized as follows. Section two provides the simulation details including a description of the force field and molecular dynamics simulation package used. In section three, simulation results on a fundamental level are presented for the thermodynamic, structural and surface energy characteristics of anatase and rutile TiO_2 nanoparticles. The results are compared for both polymorphs and important information extracted. Finally, the present work and findings are summarised and conclusions drawn in section four.

2 Simulation details

2.1 Creation of nanoparticles

The Accelrys Materials Studio 7.0 (*Materials Studio suite of crystallographic programs*) modelling package was used to create TiO_2 nanoparticles of rutile and anatase. Materials Studio is a molecular modelling package used to study and analyze models of structures at the atomic scale and provides the ability to build and represent molecular structures with enhanced graphics. Particles were constructed by initially creating an atomistic model of a perfect crystal lattice, using crystallographic information for rutile and anatase some of which are summarized in Table 1 (Naicker et al., 2005; Ahmad and Bhattacharya, 2009; Jagtap et al., 2005).

Table 1 Experimental unit cell parameters and space group for rutile and anatase (Naicker et al., 2005; Ahmad and Bhattacharya, 2009; Jagtap et al., 2005)

Phase	Crystal System	Space group	*a*, Å	*b*, Å	*c*, Å
Rutile (Sugiyama and Takéuchi, 1991)	Tetragonal	*P*42/*mnm*	4.6344	4.6344	2.9919
Anatase (Horn et al., 1972)	Tetragonal	*I*41/*amd*	3.784	3.784	9.514

Following this, the atomic coordinates for spherical arrays of atoms representing spherical particles of anatase and rutile, with diameters ranging from 2 to 6 nm, were calculated from the bulk lattice while excess surface atoms of oxygen and titanium were removed to ensure stoichiometric and electrical neutrality of the particles (Fig. 1) (Okeke et al., 2013a; Hummer et al., 2009). The choice of excess surface atoms on the spherical particles to be removed was to minimise the surface energy in vacuum of the unrelaxed particle. The sizes of the particles of anatase and rutile used in this study, and the corresponding number of TiO_2 units are given in Table 2.

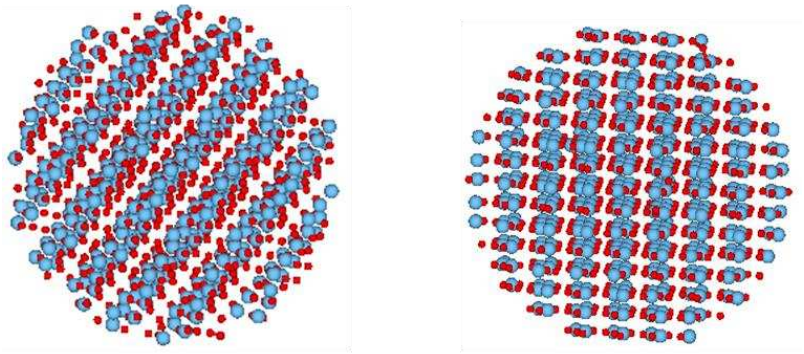

(a) (b)

Fig. 1 Image of typical structure generated for 3 nm (a) rutile and (b) anatase TiO_2 nanoparticle created using Materials Studio. Ti and O atoms are shown in red and blue colours respectively

Table 2 Size of nanoparticles (in diameter) and the corresponding number of TiO_2 units used for anatase and rutile nanoparticles

Particle size (nm)	Anatase	Rutile
2	122	126
3	415	420
4	992	980
5	1941	1918
6	3335	3304

2.2 Representation of the interatomic interactions

The force field used is the one widely reported in the literature for modelling TiO_2 polymorphs. Various articles have concluded that the Matsui – Akaogi force field (Koparde and Cummings, 2005; Filyukov et al., 2007; Koparde and Cummings, 2007; Matsui and Akaogi, 1991) is the most suitable for atomistic simulations of bulk titania polymorphs for a wide range of temperatures and when compared, outperforms other more complicated force fields (Filyukov et al., 2007; Koparde and Cummings, 2007). Whilst being a two-body, rigid-ion potential, which is relatively undemanding computationally, the Matsui – Akaogi force field reproduces the experimentally determined structures of the titania polymorphs and their order of relative stability (Koparde and Cummings, 2007). Its reliability over a range of TiO_2 configurations makes it suitable for carrying out molecular dynamics simulations at high temperatures (Collins et al., 1996). The mathematical form of the interatomic potential is as follows;

$$U(r_{ij}) = A_{ij}\, exp\left(-\frac{r_{ij}}{\rho_{ij}}\right) - \frac{C_{ij}}{r_{ij}^6} + \frac{q_i q_j}{r_{ij}} \quad (1)$$

Outside the scope of the current work, we also performed simulations by refitting the Matsui – Akaogi using additional structural data, in the form of elastic constant values, derived from DFT calculations carried out using CASTEP. The predictions of the properties from the refined force field (derived from fitting) were within reasonable limits with those predicted using the classical Matsui-Akaogi force field as well as experiments and DFT calculations from literature (Lazzeri et al., 2001; Isaak et al., 1998). Hence, for simplicity, we used Matsui-Akaogi force field in the current simulations.

For the site–site pairwise interaction $U(r_{ij})$ is the interaction energy, r_{ij} is the distance between sites *i* and *j*. The Ti and O atoms are assigned partial charges (q) of +2.196 and -1.098 respectively. The parameters A_{ij}, ρ_{ij} and C_{ij} are given in Table 3 (Oliver et al., 1997);

Table 3 Potential parameters for TiO_2. (Oliver et al., 1997)

Interaction	A_{ij} / eV	ρ_{ij} / Å	C_{ij} / eV Å^6
Ti - O	16957.53	0.194	12.59
Ti - Ti	31120.2	0.154	5.25
O - O	11782.76	0.234	30.22

Simulations were carried out for water molecules around TiO_2 nanoparticles using the three-site SPC/E (extended simple point charge) water potential (Mark and Nilsson, 2001; Okeke et al., 2012). The potential has one negatively charged site (q_{OW} = -0.8476) representing the O atoms, and two positively charged sites (q_{HW} = +0.4238) representing the H atoms (Mark and Nilsson, 2001). It can be represented in the form of Lennard Jones (LJ) potential as;

$$U(r_{ij}) = \varepsilon_{ij}\left[\left(\frac{\sigma_{ij}}{r_{ij}}\right)^{12} - 2\left(\frac{\sigma_{ij}}{r_{ij}}\right)^{6}\right] + \frac{q_i q_j}{r_{ij}} \quad (2)$$

Where σ_{ij} is the distance at which the potential has its minimum value of $-\varepsilon_{ij}$. The values of the parameters that correspond to the expression in Equation 2 are shown in Table 4. Interactions between the water molecules and TiO_2 nanoparticles were modeled using the interaction parameters (Table 4) of Bandura and Kubicki derived from ab initio calculations (Bandura and Kubicki, 2003)

Table 4 Potential parameters for SPC/E water and interaction between water molecules and TiO_2 nanoparticle interactions (Bandura and Kubicki, 2003; Mark and Nilsson, 2001)

Interaction	ε_{ij} / eV	σ_{ij} / Å	C_{ij} / eV Å^6
OW - OW	0.006738	3.166	N/A
OW - HW	0.000	0.000	
HW - HW	0.000	0.000	
Ti – OW	1239.911	0.265	6.4178

2.3 Molecular Dynamics simulation methodology

DL_POLY version 2, a classical molecular dynamics code (Koparde and Cummings, 2005; Collins et al., 1996; Alimohammadi and Fichthorn, 2009) was used to carry out the present molecular dynamics simulations. The Verlet leapfrog algorithm within DL_POLY was used to integrate Newton's equations of motion and the system temperature was maintained using the Berendsen thermostat (Smith et al., 2010). Furthermore, simulations were carried out in the canonical ensemble (NVT). The periodic, cubic simulation box used had a size that was at least 4 times larger than the diameter of the particle (Fig. 2). This was the case for all simulations and was large enough to prevent interactions between the particle and its images in the adjoining cells similar to that in a non-periodic boundary system. Simulations were carried out for 1 ns, sufficiently long to achieve a steady state in the atomic structure of the particles for a given phase. A time step of 1 fs was used in the simulations. The Ewald summation technique, as described in the DL_POLY manual (Smith et al., 2010) for molecular

simulations under periodic boundary conditions, was used in calculating the electrostatics interactions. In terms of short range interactions, a cut-off of 10Å was specified (Naicker et al., 2005), excluding all atoms outside this region including those in periodic images. In this work, size of the nanoparticles refers to their initial diameter (before simulation). Additionally, we also performed the MD simulations under non-periodic boundary conditions to make sure that the simulated generic results are not affected, significantly due to boundary condition. Unless mentioned otherwise, the simulation results reported here pertain to periodic boundary condition. In this study, temperature in the non-periodic system was maintained using the Berendsen thermostat. The electrostatic forces were calculated using the direct Coulomb summation potential.

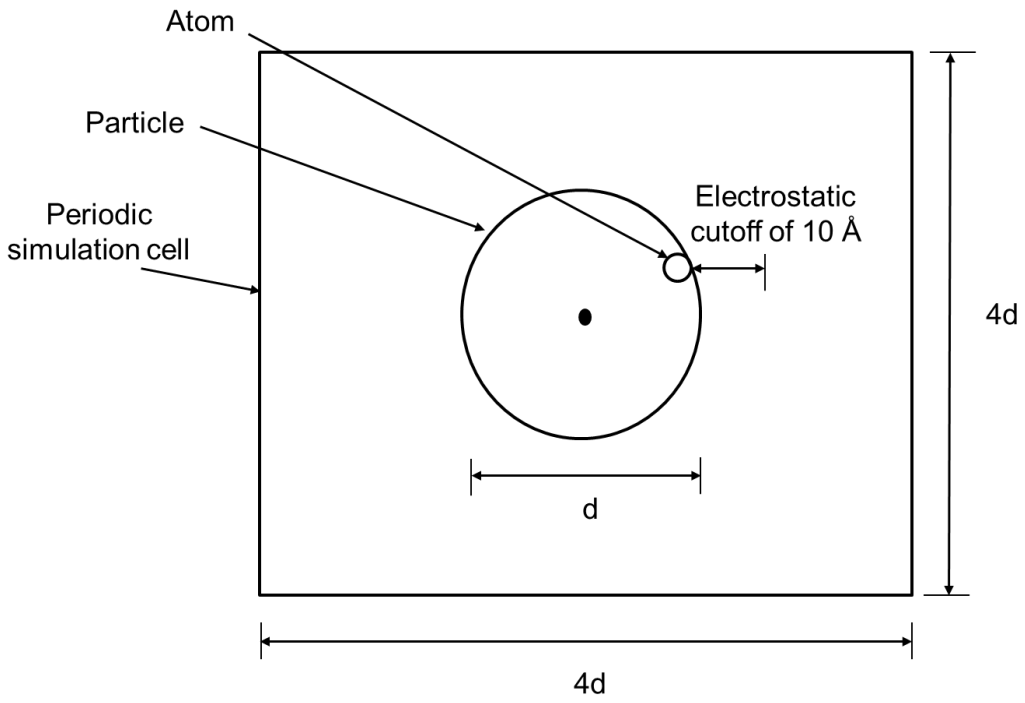

Fig. 2 Schematic diagram of a periodic simulation cell with size *4d* containing a nanoparticle of size *d*

Prior to simulations, structural optimization to obtain the minimum energy structure/local minimum, was initially carried using General Utility Lattice Program (GULP) (Gale and Rohl,

189 2003) for energy calculations of TiO_2 crystals, and DL_POLY, for energy calculations of TiO_2
190 nanoparticles using the force fields (Hummer et al., 2013).

191 3 Results and discussion

192 *3.1 Thermodynamic properties*

193 The variation of potential energy of the system, with temperature for different nanoparticle
194 sizes is shown in Fig. 3. An increase in potential energy with temperature can be observed
195 across all particle sizes. The temperature dependence of the potential energy can be used to
196 estimate the melting point of TiO_2 rutile and anatase nanoparticles. Filyukov et al.,(Filyukov
197 et al., 2007) and Collins et al.,(Collins et al., 1996) have used total energy profiles to estimate
198 the melting point and phase transition temperature of titanium dioxide microclusters of 1011
199 and 1245 atoms respectively. The number of atoms used in their work corresponds to a particle
200 diameter of about 3 nm. Filyukov et al, (Filyukov et al., 2007) estimated from their calculations
201 that the melting point for rutile and anatase is 2450 and 2250 K respectively, while Collins et
202 al, (Collins et al., 1996) estimated that the melting point for rutile clusters was in the range
203 from 2150 to 2300 K. In Fig. 3, the rate of change of potential energy with temperature for
204 both rutile and anatase is seen to increase linearly with increasing temperature for all particle
205 sizes. Apart from the case of a particle diameter of 2 nm, this trend is seen to be associated
206 with a sudden steep increase in the rate of change of potential energy at a particular
207 temperature, which represents the melting transition. The melting transition is characterised
208 by a temperature range with bounds which can be considered as lower and upper bounds.
209 Following the sudden steep increase in the rate of change of potential energy for a temperature
210 range which represents the melting transition, the energy increases linearly with a decreasing
211 rate. It can also be observed that generally, anatase melts at a lower temperature except for 2
212 nm particle sizes, compared to rutile. In the case of 3 and 4 nm, the change in energy gradient

associated with the melting transition is seen to occur between a temperature of 1500 and 2000 K for anatase, and 2000 and 2500 K for rutile. For 5 nm, this transition is seen to occur between 2000 and 2500 K for both rutile and anatase. However, for 6 nm, the transition is seen to occur between a temperature of 2000 and 2500 K for anatase, and 2500 and 3000 K for rutile. It can be further observed that the temperature associated with the melting transition increases with increasing particle size. Takagi, (Takagi, 1954) was the first to study the size dependence of very small particles of tin on melting, through experiments (Skripov et al., 1981). Takagi detected the melting of thin layers of tin using the reflection electron diffraction technique and took the radii of the spherical tin particles in the layers to be equal to the mean thickness of the layers (Wronski, 1967). Takagi observed that the melting points of the small particles ranging from 10 to 1000 Å were lower than those of bulk metals. Following this observation, he calculated the melting temperature as a function of crystal size, and found that experimental results were in fairly good agreement with the results from calculations. The size effect of TiO_2 nanoparticles on their melting temperature has also been investigated theoretically by Mishra et al, (Mishra et al., 2012) using Arrhenius relation and Lindemann's criteria assuming that the melting point of the nanoparticles decreases with decrease in size of the nanoparticles, as evident from the current MD simulations. Though their theoretical analysis accounted for the size effects of titania nanoparticles, the phase effects were not accounted explicitly unlike in the current MD simulations.

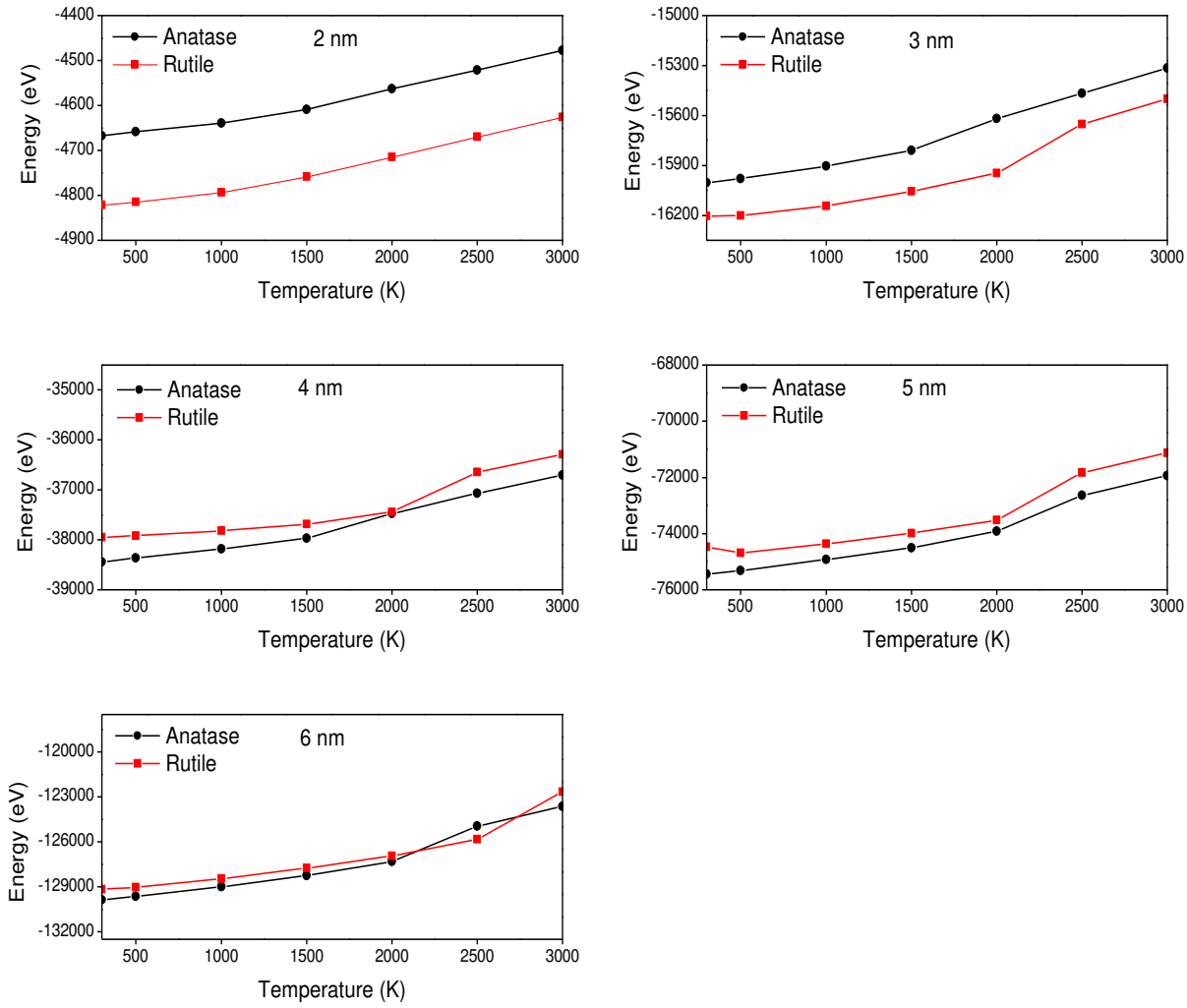

Fig. 3 Potential energy as a function of temperature for 2 – 6 nm size nanoparticles for simulation in periodic boundary condition

We also observed that the potential energy change associated with the melting transition for anatase seems to be less than for rutile nanoparticles. This suggests that for nanoparticles of the current size range, rutile is the more thermal stable phase as its melting transition occurs at higher temperatures compared to anatase.

To further confirm our system was similar to that of a non-periodic system, some test simulations were conducted and thermodynamic results (Fig. 4) for both systems compared. It can be observed the variation of potential energy with temperature in both systems, is fairly similar across all particle sizes. Hence, this established a basis to conduct simulations in non-

periodic condition, in this study. For brevity, hereafter we present the results pertaining to periodic boundary conditions.

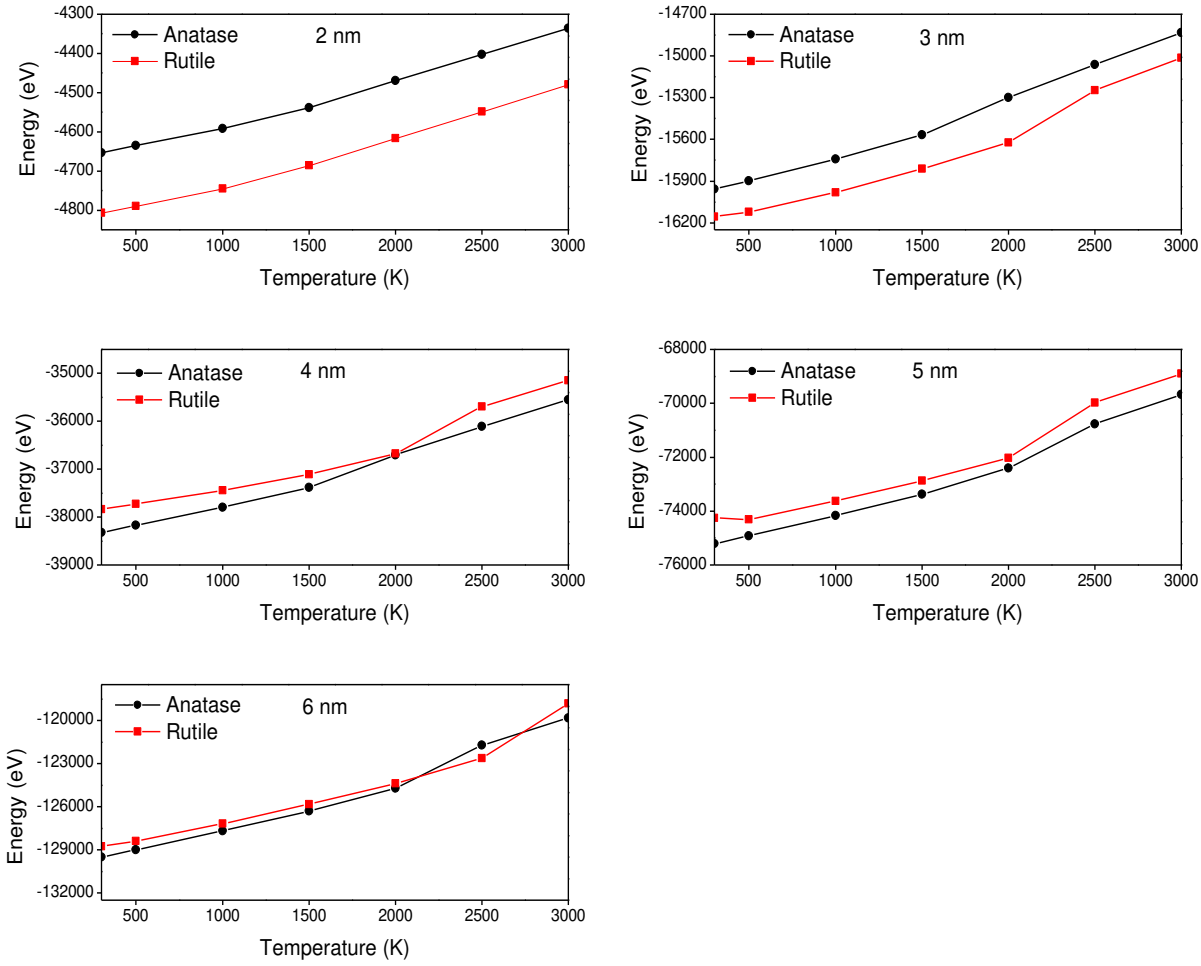

Fig. 4 Potential energy as a function of temperature for 2 – 6 nm size nanoparticles for simulation in non-periodic boundary condition

3.2 Structural properties

Radial distribution functions (RDFs) describe the variation of atomic density as a function of the distance from a reference atom and therefore represent the structure of liquid and solid phases (Brostow, 1977). They are useful for describing the time-averaged, local coordination around a specific atom-type and are indicative of a material's internal structure. The function $G(r)$, represents the probability of locating an atom at a distance r from a reference atom (in our case the centre atom of the particle), compared to a homogenous material such as an ideal

gas, of the same number density. The function $G(r)$ can be used to estimate the coordination number $n_{ij}(r)$ for specific atomic-sites in a structure (Brostow, 1977). The coordination number of a central/reference atom represents the number of its nearest neighbours which, as a structural parameter, is used in structural analysis. As this number captures the number of nearest neighbour atoms bonded to a central atom, it is also associated to the bond length. The coordination number, $n_{ij}(r)$ is given by the following equation (Brostow, 1977);

$$n_{ij}(r) = 4\pi\rho \int_{r_{min}}^{r_{max}} r^2 G(r) dr \tag{3}$$

Where ρ is the number density and is given as; $\rho = N/V$ in which case N is the number of atoms/molecules in a system of volume V.

Typical RDF plots for 3 nm anatase and rutile are shown for Ti – Ti, Ti – O and O – O pairs at temperatures between 300 and 3000 K are shown in Fig. 5 and 6. For the purpose of determining the coordination number of Ti atoms, a cut-off radius, which describes the number of oxygen atoms in the cut-off region, was set to 2.3 Å. In the context of the RDF plot, the cut-off radius represents the position of the first minimum after the first peak (r_{min} is the lower limit before the first peak and r_{max} is the upper limit after the first peak) (Hines et al., 1985; Brostow, 1977). Based on this, the coordination numbers of Ti for the different particle sizes and temperatures are reported in Table 5.

Table 5 Coordination number for corresponding particle size, initial bond length (before simulation), $\boldsymbol{r_{ij}}$, and temperature for anatase and rutile TiO_2 nanoparticles (Okeke et al., 2013b)

Anatase								
Particle size (nm)	$\boldsymbol{r_{ij}}$ **(Å)**	$\boldsymbol{n_{ij}(r)}$						
		Mostly ordered state				**Transition state**		**Liquid state**
	Ti - O	**300 K**	**500 K**	**1000 K**	**1500 K**	**2000 K**	**2500 K**	**3000 K**
2	1.89	5.33	5.31	5.22	5.01	4.78	4.58	4.38
3	1.91	5.48	5.48	5.41	5.27	4.96	4.72	4.50
4	1.91	5.62	5.60	5.53	5.42	5.06	4.79	4.56

5	1.91	5.68	5.68	5.61	5.52	5.32	4.83	4.60
6	1.91	5.72	5.72	5.67	5.58	5.40	4.85	4.61
Rutile								
Particle size (nm)	**r_{ij} (Å)**	**$n_{ij}(r)$**						
		Mostly ordered state				**Transition state**		**Liquid state**
	Ti - O	**300 K**	**500 K**	**1000 K**	**1500 K**	**2000 K**	**2500 K**	**3000 K**
2	1.89	5.31	5.38	5.24	5.11	4.88	4.69	4.50
3	1.91	5.61	5.54	5.43	5.37	5.17	4.72	4.50
4	1.91	5.91	5.62	5.56	5.50	5.36	4.82	4.59
5	1.91	5.69	5.68	5.64	5.60	5.48	5.24	4.70
6	1.91	5.74	5.72	5.69	5.62	5.49	5.26	4.79

Table 5 also provides the bond length for both anatase and rutile nanoparticles of 1.89 Å for 2 nm particle size while a bond length of 1.91 Å is seen for particle sizes between 3 and 6 nm (Naicker et al., 2005). These results are consistent with molecular dynamics simulation results reported in the literature (Naicker et al., 2005) which suggest that 5-coordinated titanium has an associated bond length of 1.92 Å. The RDF at 3000 K best describes a molten TiO_2 system. The melting point of rutile and anatase titania, is 2450 and 2250 K respectively, widely reported in literature (Collins et al., 1996; Filyukov et al., 2007) falls within the high temperature region in Table 5, where the coordination number is seen to drop from 5 to 4 (indicating under-coordination) especially at smaller particle sizes. The bond length for Ti – O in anatase observed here is in agreement with previous studies (Tang et al., 1993; Zhang et al., 2008; Banfield et al., 1993) in which a coordination number of 5.3 is reported which suggests a mixture of Ti – O octahedra and pentahedra having coordination numbers of 6 and 5 respectively. It can be observed from Table 5 that the system becomes tetrahedrally coordinated (i.e. 4-coordinated titanium) as the temperature increases in transition state, the coordination number increases with increasing particle size and decreases with increasing temperature. The tetrahedrally coordinated titanium represents undercoordinated TiO_n units (where $n < 6$) such as those present in Ba_2TiO_4 where the Ti – O bond length varies between 1.63 and 1.82 Å (Hoang, 2008). This tetrahedral coordination of titanium is thought to characterise liquid TiO_2 systems (Hoang, 2008). In addition, tetrahedral coordination of

titanium is observed in the temperature range from 2000 to 3000 K for all the particle sizes investigated. These observations correspond to the thermodynamic properties of the anatase and rutile particles where it is seen that the melting point is approached at temperatures between 2000 and 2500 K after which the system is observed to become more liquid-like.

The RDFs in Fig.s 5 - 8 represent a range of structural configurations for anatase and rutile for typical cases of 3 and 6 nm nanoparticles. For other particle sizes, the generic results were identical and not repeated here. The RDF's change from well-ordered to molten configuration for increasing temperature. The well-ordered configuration is characterised by a profile which manifests a greater number of narrower peaks (for temperatures below 2000 K) with increasing radius. The molten configuration is characterised by a profile with both fewer and broader peaks (for temperatures above 2000 K). The plots were generated from the time-average RDF values over the entire simulation. The greater order, in the case of the lowest temperature (300 K) can be attributed to the higher coordination number of titanium. It is observed that the peaks for each atom pair broaden as the temperature increases. The initial double peaks observed in the Ti – Ti and O – O RDF's is seen to broaden as the temperature is increased. Initially at 300 K, the structure is highly crystalline and well ordered. The degree of order decreases with increase in temperature and the peaks reduce in intensity for high temperatures of 3000 K where the structure is observed to be more liquid-like. The same general trends were observed for other particle sizes of this study though not presented here.

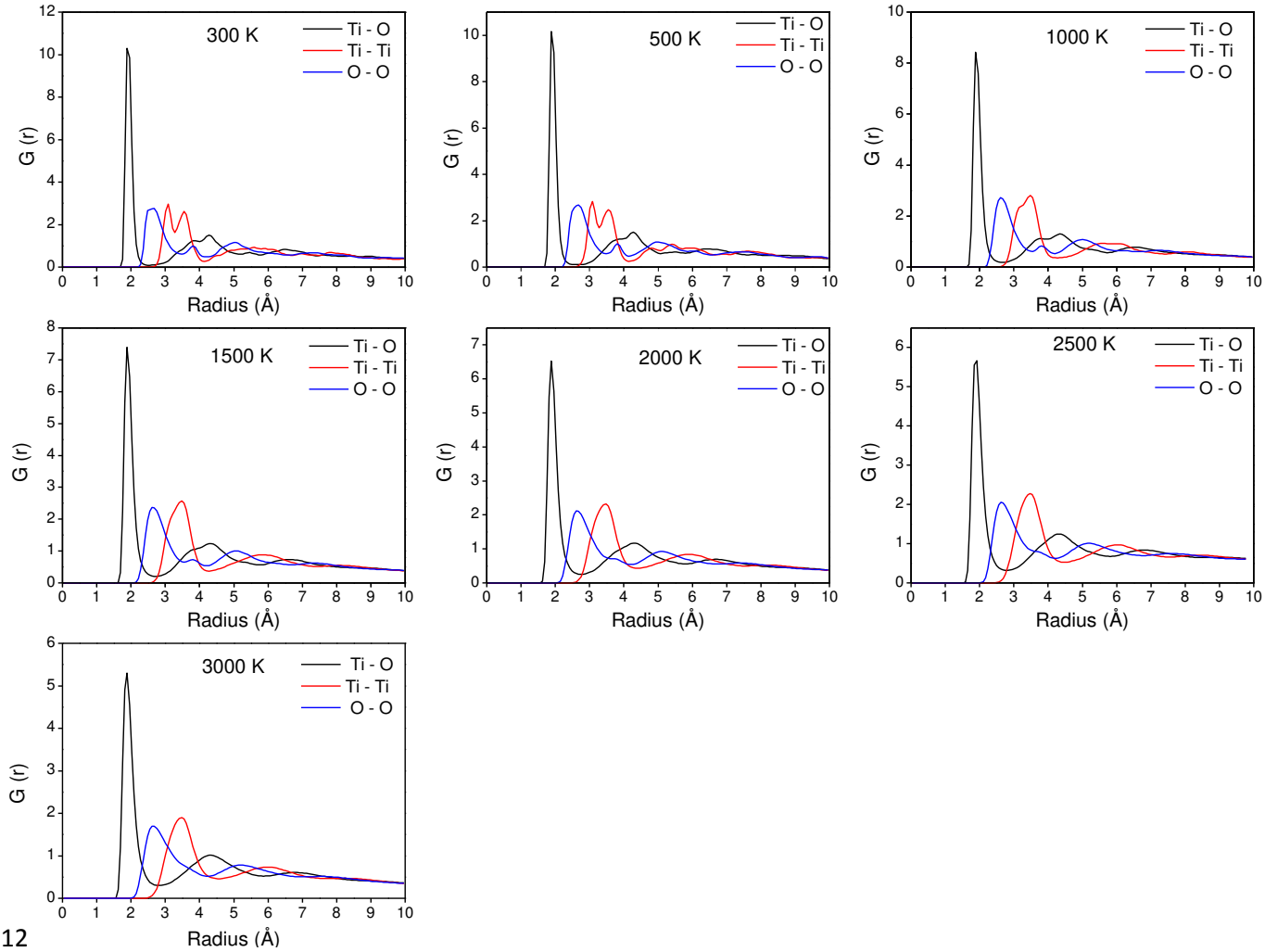

Fig. 5 RDF's for anatase Ti – Ti, Ti – O and O – O pairs for 3 nm

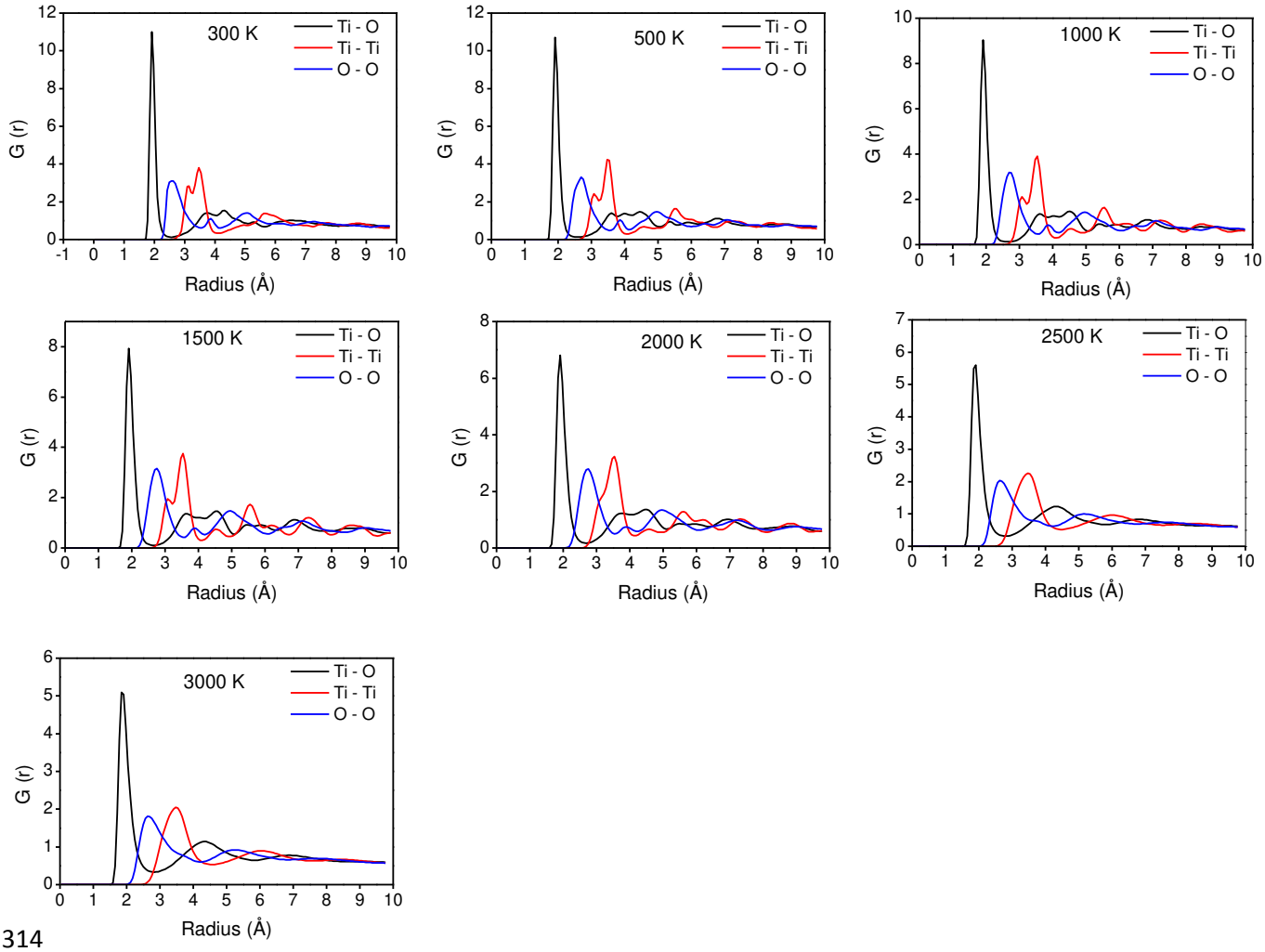

Fig. 6 RDF's for rutile Ti – Ti, Ti – O and O – O pairs for 3 nm

The RDF trends for both anatase and rutile can be linked to the variation of potential energy of the system with temperature as observed in Fig. 3. In Fig. 3, it can be observed that the change in energy gradient associated with the melting transition occurs at almost similar temperatures to the temperatures associated with the stretching and broadening of RDF's in Fig. 5 and 6. In the case of 3 nm, the melting transition in Fig. 3 occurred between 1500 and 2000 K for anatase, and 2000 and 2500 K for rutile, and is similar to the temperature at which the stretching and broadening of the RDF's begin to occur, in Fig. 5 and 6. Similarly, for 6 nm, the melting transition in Fig. 3 occurred between 2000 and 2500 K for anatase, and at 3000 K for rutile. This can be compared to the temperature at which the RDF's begin to stretch in Fig. 7 and 8, as stretching begins to occur from 2500 K for anatase, and 3000 K for rutile.

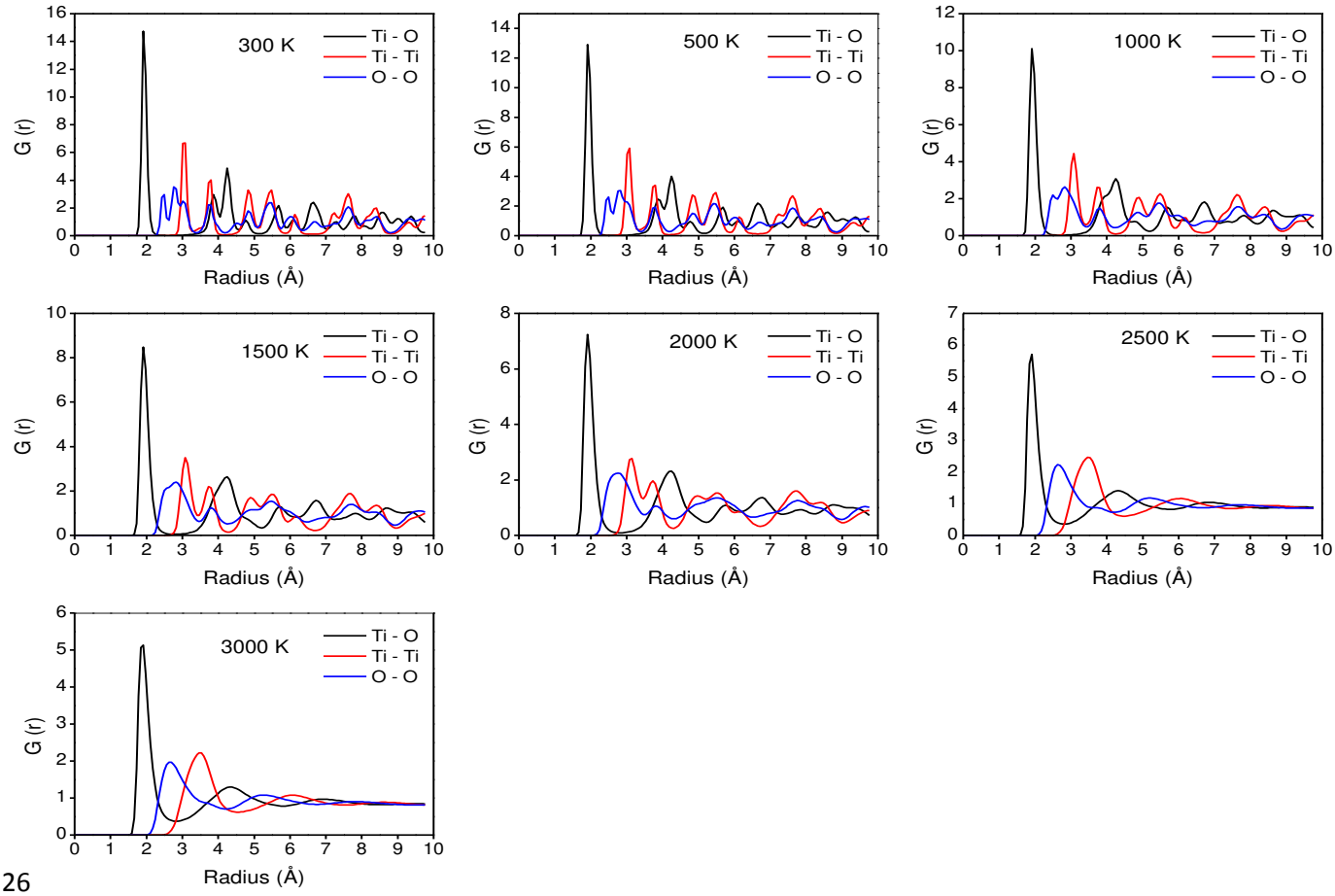

326

327 **Fig. 7** RDF's for anatase Ti – Ti, Ti – O and O – O pairs for 6 nm

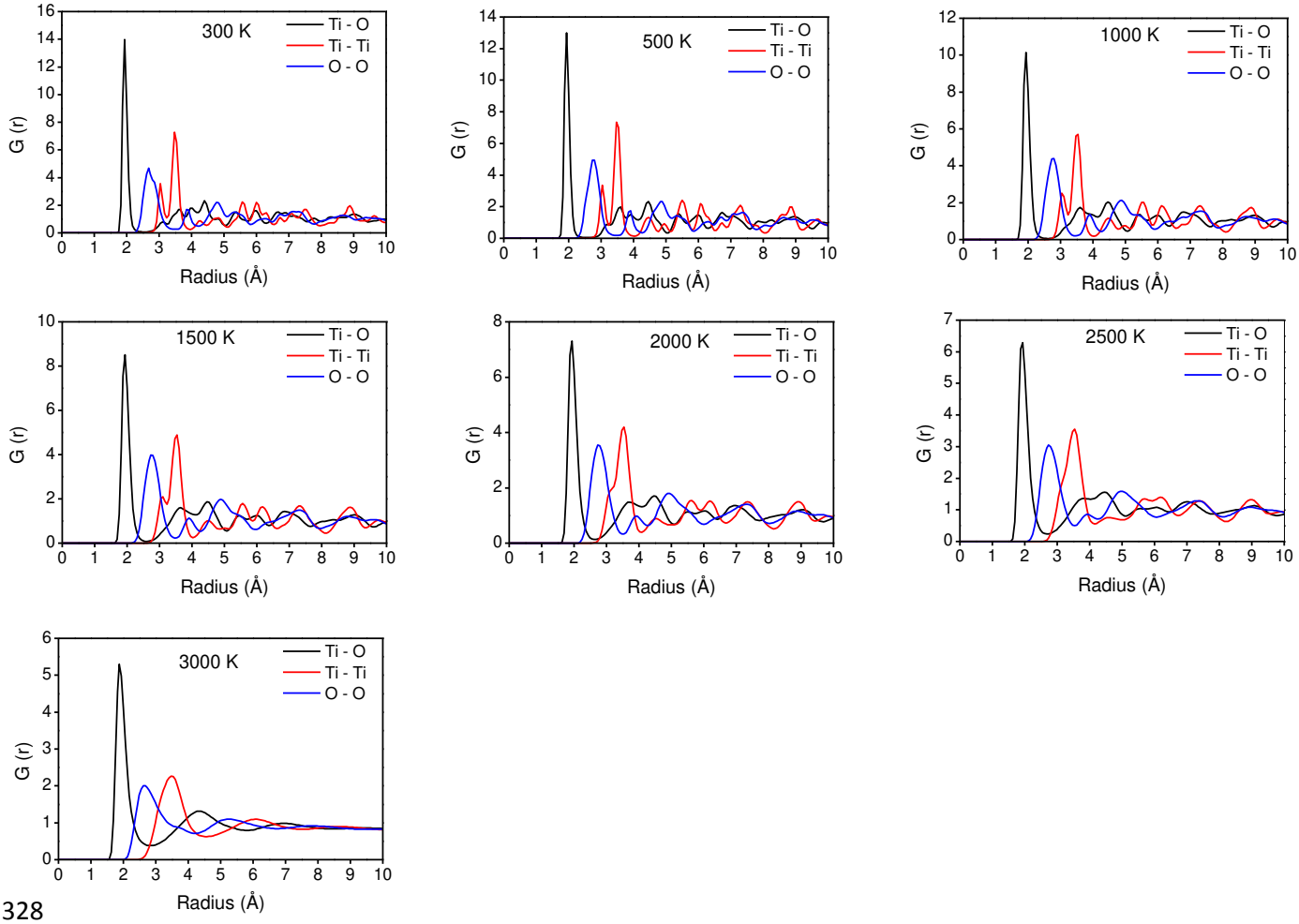

328

329 **Fig. 8** RDF's for rutile Ti – Ti, Ti – O and O – O pairs for 6 nm

330 Overall, the temperature (which represents the melting transition) at which the RDF's begin to
331 stretch and broaden is observed to be lower for the case of anatase, compared to rutile. This
332 further suggests that rutile is the more stable phase for nanoparticles within the size range in
333 this study, and is similar to the concluding observations in the preceding thermodynamic
334 section.

335 ### *3.3 Surface energy*

336 #### *3.3.1 TiO_2 crystals*

337 Models of crystal morphology are often calculated based on surface energy term which is
338 defined in Equation 3, and is taken to represent crystals grown under a minimum driving force
339 i.e. at conditions close to thermodynamic equilibrium. Given a bulk energy of U_{bulk}, an energy

for a surface created in the same system, $U_{surface}$, and a surface area A, the surface energy ΔU_{SE} can be defined as(Gale and Rohl, 2003);

$$\Delta U_{SE} = \frac{(U_{surface} - U_{bulk})}{A} \quad (4)$$

In this work, surface energy of the crystalline structures of anatase and rutile were obtained using the molecular modelling code, GULP (Gale and Rohl, 2003). Furthermore, the center-face distances between the center of the crystal and its individual surfaces, were scaled to be proportional to the surface energies of the surfaces. Hence, crystal surfaces with low surface energies would experience more growth compared to surfaces with high surface energies.

Surface energies for anatase and rutile crystals have been reported in Table 6. Similar calculations have been previously presented by Oliver et al, (Oliver et al., 1997) for the bulk crystals of TiO_2, which are in a reasonable agreement with the current work. Results show that rutile has higher surface energies for both the unrelaxed and relaxed surfaces. For example, surface energies for the (0 0 1) and (1 0 0) surfaces of anatase are 1.30 and 2.28 Jm^{-2} respectively, while those for rutile are 2.83 and 4.43 Jm^{-2} respectively.

Table 6 Surface energies for rutile and anatase calculated using GULP (0 K)

Surface (*hkl*)	**Unrelaxed (Jm^{-2})**		**Relaxed (Jm^{-2})**	
	Rutile	**Anatase**	**Rutile**	**Anatase**
(1 1 0)	2.07	2.91	1.79	2.26
(0 1 1)	2.08	1.67	1.86	1.41
(1 0 0)	2.43	2.28	2.10	1.69
(1 2 1)	4.57	-	2.16	-
(0 0 1)	2.83	1.30	2.42	1.30
(2 2 1)	3.77	-	2.12	-
(1 2 0)	-	2.83	-	2.12

Models of the equilibrium crystal morphology for anatase and rutile are presented in Fig. 9, and have been predicted using the computed surface energies summarized in Table 6, both at 0

K. The (1 1 0), (0 1 1), and (1 0 0) surfaces are expressed in the unrelaxed rutile surfaces. The (2 2 1) surface is expressed in the relaxed rutile morphology and is mainly due to the reduction in its surface energy upon relaxation from 3.77 Jm^{-2} to 2.12 Jm^{-2}. The capped octahedral shape observed in the anatase morphologies is as a result of the (0 1 1) octahedral form which is capped with the (0 0 1) surface. Anatase showed the least change in surface energy when comparing the unrelaxed to the relaxed surfaces. It can be observed from Table 6 that the amount of change between the unrelaxed and relaxed morphologies is much smaller in the case of anatase when compared with that of rutile. This could be attributed to possibly more stability of anatase phase in crystalline form (Zhang and F. Banfield, 1998). We wish to point out that the surface energy data derived from experiments for rutile and anatase TiO_2 nanoparticles are limited at this time. However, our surface energies for different crystal surfaces were used to predict the equilibrium morphology of rutile and anatase. The predicted morphologies (Fig.9) are similar to those presented from experiments (Oliver et al., 1997).

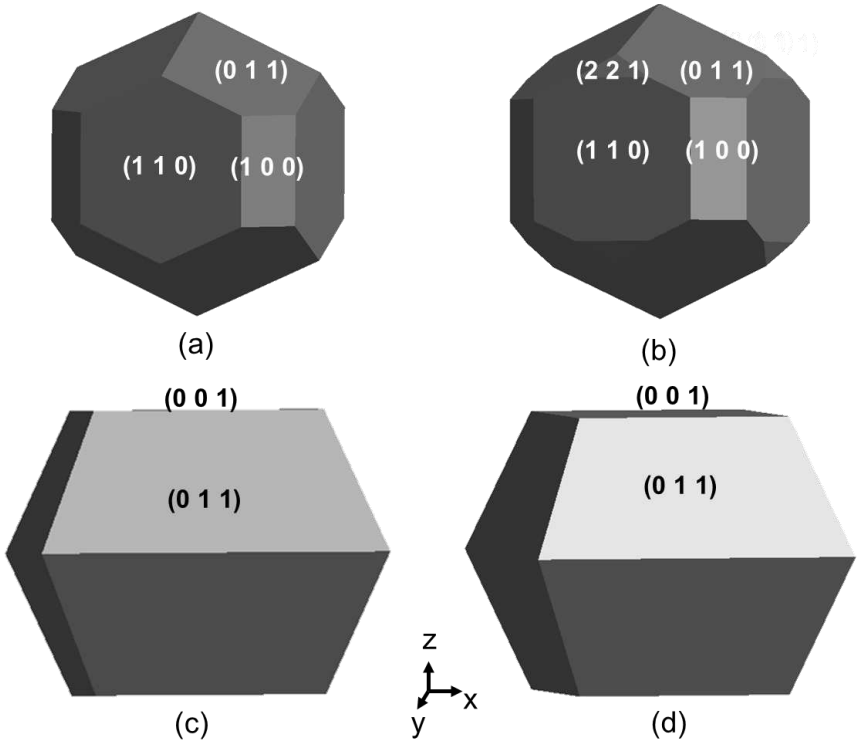

Fig. 9 Prediction of the calculated equilibrium morphology using surface energies for (a) unrelaxed rutile, (b) relaxed rutile, (c) unrelaxed anatase, (d) relaxed anatase

3.3.2 *TiO_2 nanoparticles*

Surface energy of TiO_2 nanoparticles was calculated using the following expression (Naicker et al., 2005; Song et al., 2009)

$$\Delta U_{SE} = \frac{(U_{cluster} - nU_{bulk})}{4\pi r^2} \quad (5)$$

Where $U_{cluster}$ is the potential energy of the nanoparticle, U_{bulk} is the potential energy per TiO_2 unit in the bulk material, n is the number of TiO_2 units in the nanoparticle and r is the radius of the nanoparticle. The surface energy of nanoparticles is estimated by including any differences between the energy of atoms in the interior of the nanoparticle, and those in the crystalline material. Therefore, it is necessary to calculate the energy of the bulk material in such a way as to minimise any effects due to change in shape of particle surfaces as a result of these energy differences. In this work, surface energy of the nanoparticles was calculated at different temperatures ranging from 300 – 2500 K. The energy of the bulk material, U_{bulk}, was calculated at the required temperatures (corresponding to the temperatures employed in the molecular dynamic simulations) of the nano-particles. Since the particles become less spherical as temperature increases, the assumption that the particle is spherical and hence the use of the formula for surface area (i.e. $4\pi r^2$) in Equation 4 becomes a poor approximation. For this reason, actual surface-area values for the particles were obtained from Materials Studio. Materials Studio estimates the surface area by creating a Connolly, van der Waals or solvent surface around the material (treated at the atomic scale), depending on the choice of surface. In this case, surface area calculations were made using the Connolly surface (Connolly, 1983).

Surface energies of anatase and rutile for different particle sizes at 300 K are reported in Fig. 10. We examined the standard deviations in the potential energies by repeating the simulations

3 times and the surface energies were accurate within 0.02 Jm^{-2}. This has been further validated with surface energy data reported by Naicker et al, using MD simulations at 300 K (Naicker et al., 2005). The plots show that the surface energy of anatase from Naicker et al., (Naicker et al., 2005) is slightly higher than that found in the present study by about 5 % which is reasonable given the inherent accuracy of the calculation approach. Surface energy results also show a significant rise in energy for increasing particle size until a maximum is reached, and then no further increase is observed. For rutile, the surface energy reported in the literature (Naicker et al., 2005) for room temperature is higher by about 13 – 16 % between 2 and 4 nm (Fig. 10). For particles with a diameter greater than 4 nm, the surface energy reported by Naicker et al. is in reasonable agreement (i.e. surface energy within about 0.3 – 1.2 %). The observed difference between the data set of Naicker et al.,(Naicker et al., 2005) and the present study could be due to the fact that their surface energy calculations were based on the assumption that the nanoparticles remain spherical during simulations as defined by Equation 5. However, by calculating the particle surface-area from the Connolly surface (Connolly, 1983) in the present study, any effect from a change in the shape of the particles, including faceting, is taken into account.

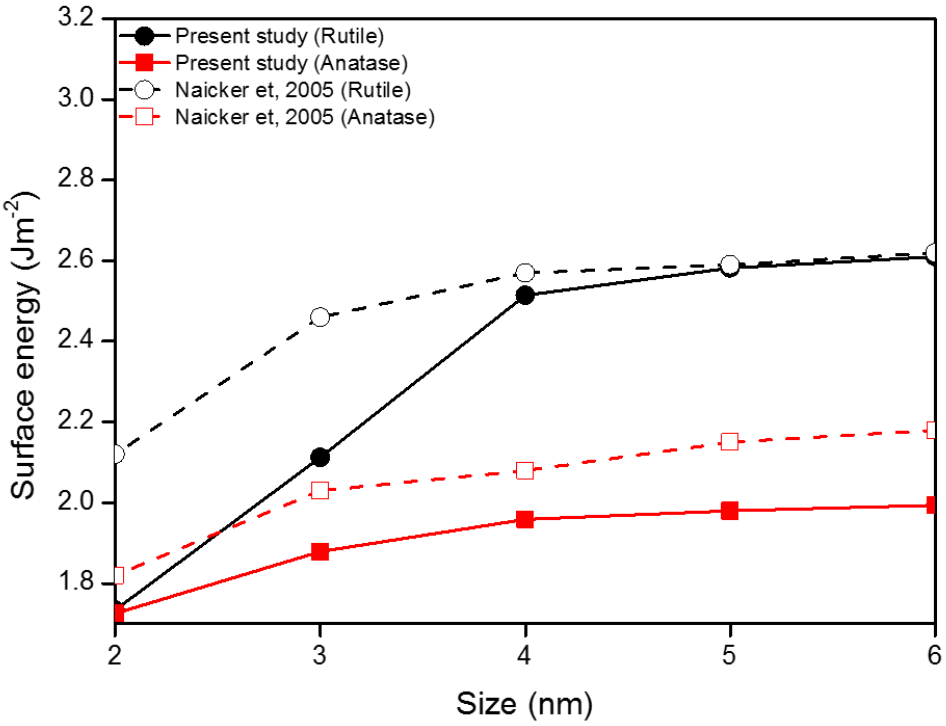

411

412 **Fig. 10** Surface energy of anatase and rutile nanoparticles from present study and literature at

413 300 K

414 Fig.s 11 and 12 show structural changes in anatase and rutile nanoparticles respectively after

415 MD simulations at temperatures between 300 and 3000 K. In the case of anatase, it can be

416 seen that the change is more evident for a particle size of 2 nm (top row in Fig. 11), and reduces

417 to a minimum for a particle size of 6 nm (bottom row in Fig. 11). The particles tend to retain

418 their sphericity more as the particle size increases, especially below the transition temperature

419 regime. However, this is not the case with rutile as the particles become non-spherical and

420 more oval shaped (as a nanorod) as the particle size increases (Fig. 12).

Size (nm)	Before simulation	Simulations at						
		300 K	500 K	1000 K	1500 K	2000 K	2500 K	3000 K
2	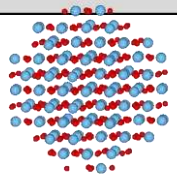	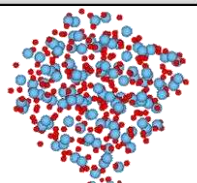	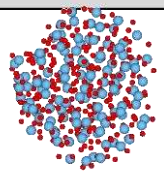	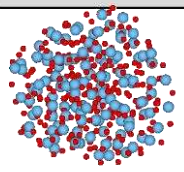	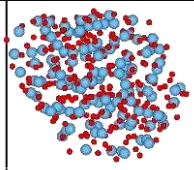	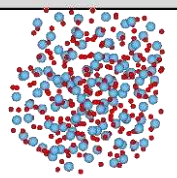	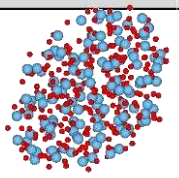	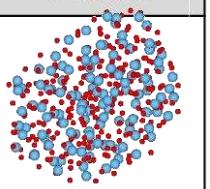
3	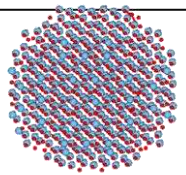	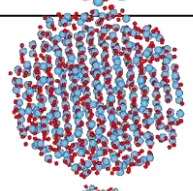	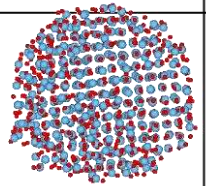	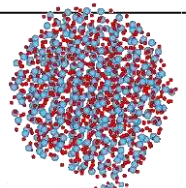	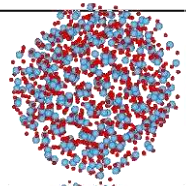	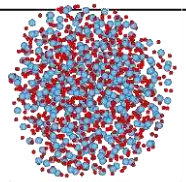	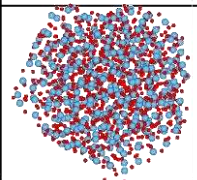	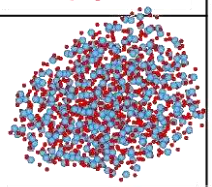
4	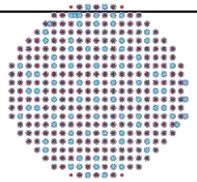	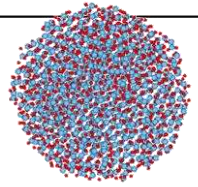	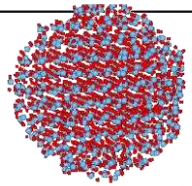	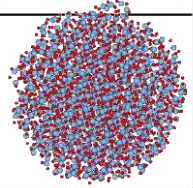	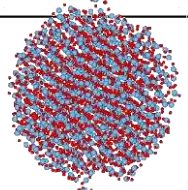	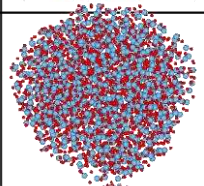	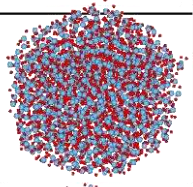	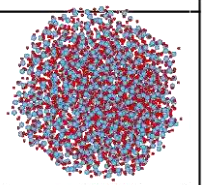
5	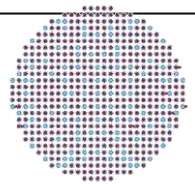	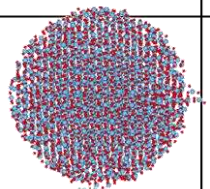	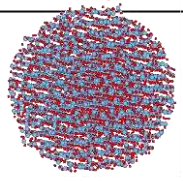	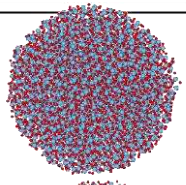	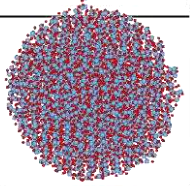	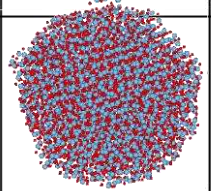	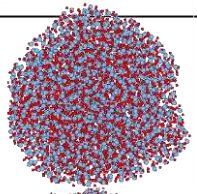	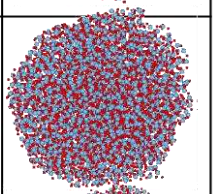
6		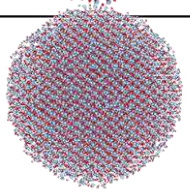	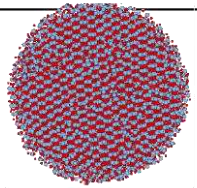	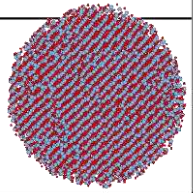	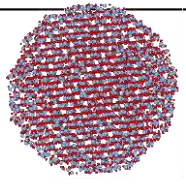	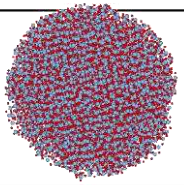	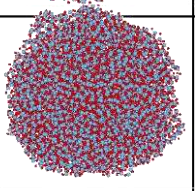	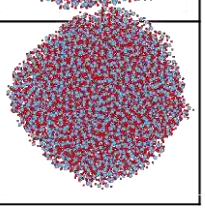

Fig. 11 Structural change of anatase nanoparticles before and after MD simulation at different temperatures. Ti and O atoms in red and blue colours respectively

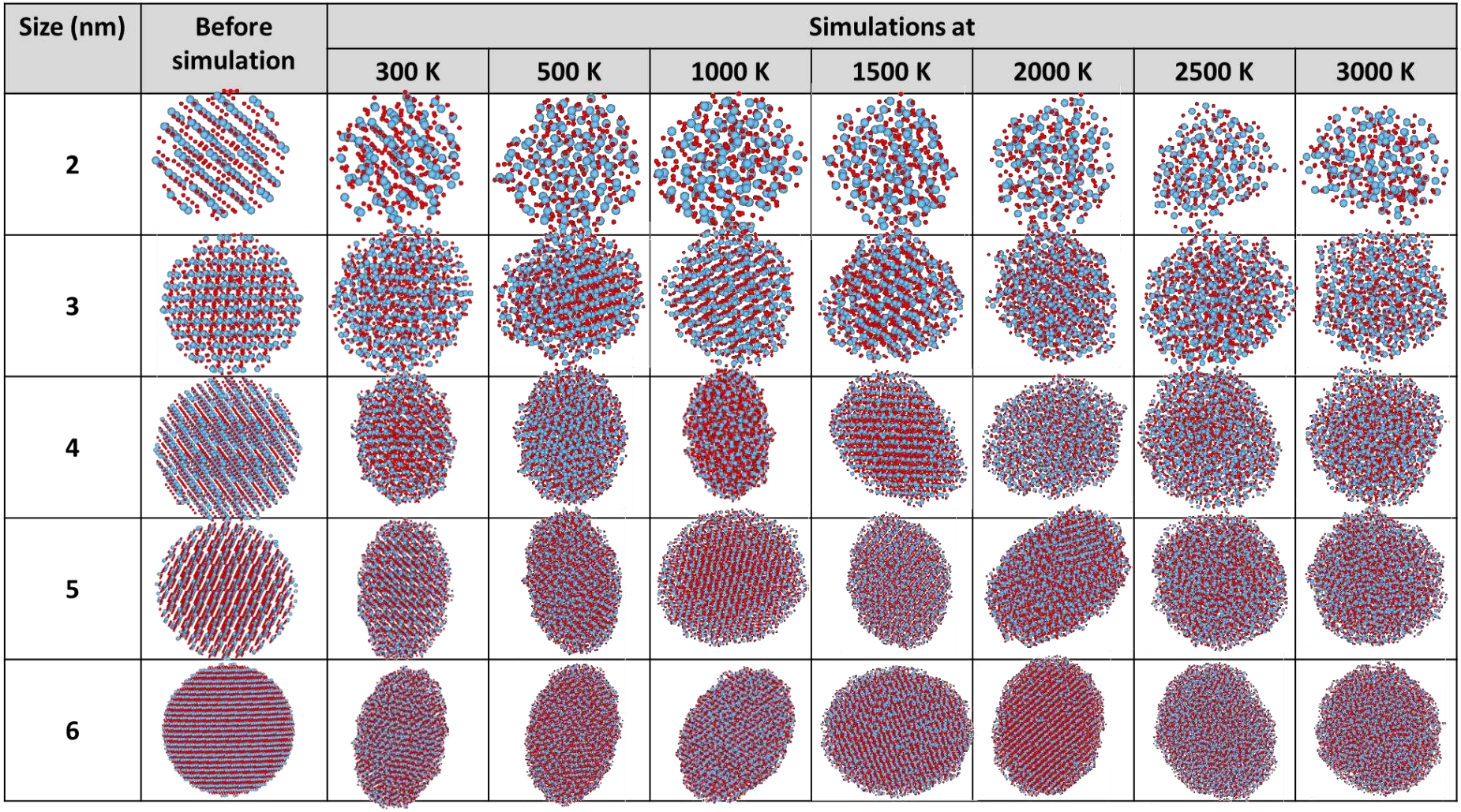

Fig. 12 Structural change of rutile nanoparticles before and after MD simulation at different temperatures. Ti and O atoms in red and blue colours respectively

Notice that 2 and 3 nm rutile nanoparticles in Fig. 12 are still somewhat spherical after simulation mostly at temperatures between 300 and 1500 K. However, there is a significant change at particle diameters of 4 to 6 nm as particles tend to become nanorods especially below the molten temperature. This may be related to the trend in the surface energy plot for rutile in Fig. 10. A change in the surface energy is observed from 4 nm for increase in particle size. The increase in surface disordering observed for both anatase and rutile nanoparticles as temperature increases, is also manifested in the RDF plots of Figures 5 - 8. Reyes-Coronado et al., (Reyes-Coronado et al., 2008) have experimentally studied anatase and rutile nanoparticles using TEM, following the hydrothermal treatment of these particles at 200^0C for a period of 48 hours. They confirmed that upon treatment, the anatase nanoparticles showed a well-faceted crystal habit. In the case of rutile nanoparticles, they observed that after treatment for a period of 5 hours at 200^0C, the particles were seen to organise as nanorods, and oriented to form larger aggregates in the form of nanorods. The nanorods, showed the (0 1 1) and (1 0 0) surface planes. Ribeiro et al., (Ribeiro et al., 2007) also carried out characterisation of anatase and rutile nanoparticles following hydrothermal treatment at 95^0C for a period of 48 hours. Using TEM, they observed that while anatase nanoparticles were bipyramidal in shape, the rutile nanoparticles were rod-like. They also confirm that the (1 1 0) planes are predominant in the rutile morphology, as a result of their low surface energy. Fig. 13 shows their TEM images of typical rutile nanorods(Ribeiro et al., 2007). These observations are in line with the shape of rutile obtained in the current MD simulations as shown in Fig. 12, which takes a rod-like form at ambient temperature (300 K) and below the melting temperature (transition regime).

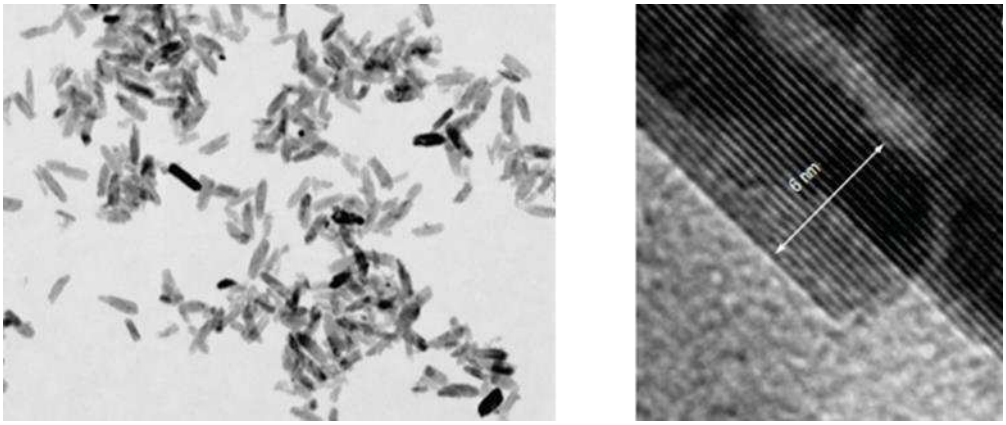

448

449 **Fig. 13** TEM images showing rutile TiO_2 nanorods (Ribeiro et al., 2007).

450

451 Interestingly, the observed degree of change of particle shape is less in anatase compared to
452 rutile (i.e. as seen when comparing Fig. 11 to 12). For example, in the case of 6 nm at 300 K,
453 the change in sphericity of the anatase particles is about 6 % while that of rutile is about 10 %.
454 It has been reported (Reyes-Coronado et al., 2008) that nanocrystalline rutile tends to grow
455 mostly in the [1 1 0] direction at elevated temperatures, thereby making the crystals take the
456 shape of nanorods. The (1 1 0) are the lower energy planes in rutile and show predominance
457 amongst the other rutile planes, minimizing the total surface energy of the rod. Overall,
458 observations in Fig.s 11 and 12 suggest that non-spherical TiO_2 particles at the nanoscale in
459 rutile phase tends to be thermodynamically more stable (also reflected in their RDF's, Fig.s 5
460 – 8).

461 Surface energy values of TiO_2 nanoparticles at 300 K are shown in Table 7. In both cases of
462 TiO_2 crystalline and nanoparticles, the surface energy of rutile is seen to be higher than that of
463 anatase. It can be observed that the surface energy values of both nanoparticle polymorphs are
464 in reasonable agreement with those of the crystal surfaces presented in Table 6.

465

466

467 **Table 7** Surface energy (in Jm^{-2}) of rutile and anatase nanoparticles at 300 K

Diameter (nm)	Rutile (Jm^{-2})	Anatase (Jm^{-2})
2	1.73	1.72
3	2.11	1.87
4	2.51	1.95
5	2.58	1.98
6	2.61	1.99

468 The mean surface energy of anatase nanoparticles in the size range between 2 and 6 nm in
469 diameter is 1.90 Jm^{-2} while that for the relaxed crystal surfaces from the present study is 1.76
470 Jm^{-2}. Similarly, the mean surface energy of rutile nanoparticles between 2 and 6 nm is 2.28 Jm^{-2}
471 while that for the crystal surfaces from the present study is 2.08 Jm^{-2}. Overall, the surface
472 energies of rutile and anatase surfaces in Table 5 are within the range of 1.30 and 2.42 Jm^{-2}
473 with the (1 1 0) and (0 0 1) surfaces having the lowest surface energy for the rutile and anatase
474 phases, respectively. These surface energy values compare reasonably well with those for the
475 rutile and anatase nanoparticles. Considering the fact that the crystal surfaces investigated in
476 this work are the low index surfaces, this suggests that nanoparticles of both rutile and anatase
477 phases are mostly dominated by low index crystal surfaces. These low index surfaces are
478 known to be the most stable surfaces (Oliver et al., 1997).

479 Surface energies for anatase and rutile at different temperatures and as a function of particle
480 size, are reported and compared in Fig. 14. Surface energies for anatase particles at 300, 1000
481 and 1500 K are seen to increase to a maximum at 4 nm size after which no further significant
482 increase is observed. It is also worth noting that for particle size at and beyond 4 nm, rutile
483 nanoparticles are strongly non-spherical in shape. This change in shape is triggered at lower
484 temperatures in the case of rutile nanoparticles, whereas in anatase, this generally occurs at
485 higher temperatures.

486

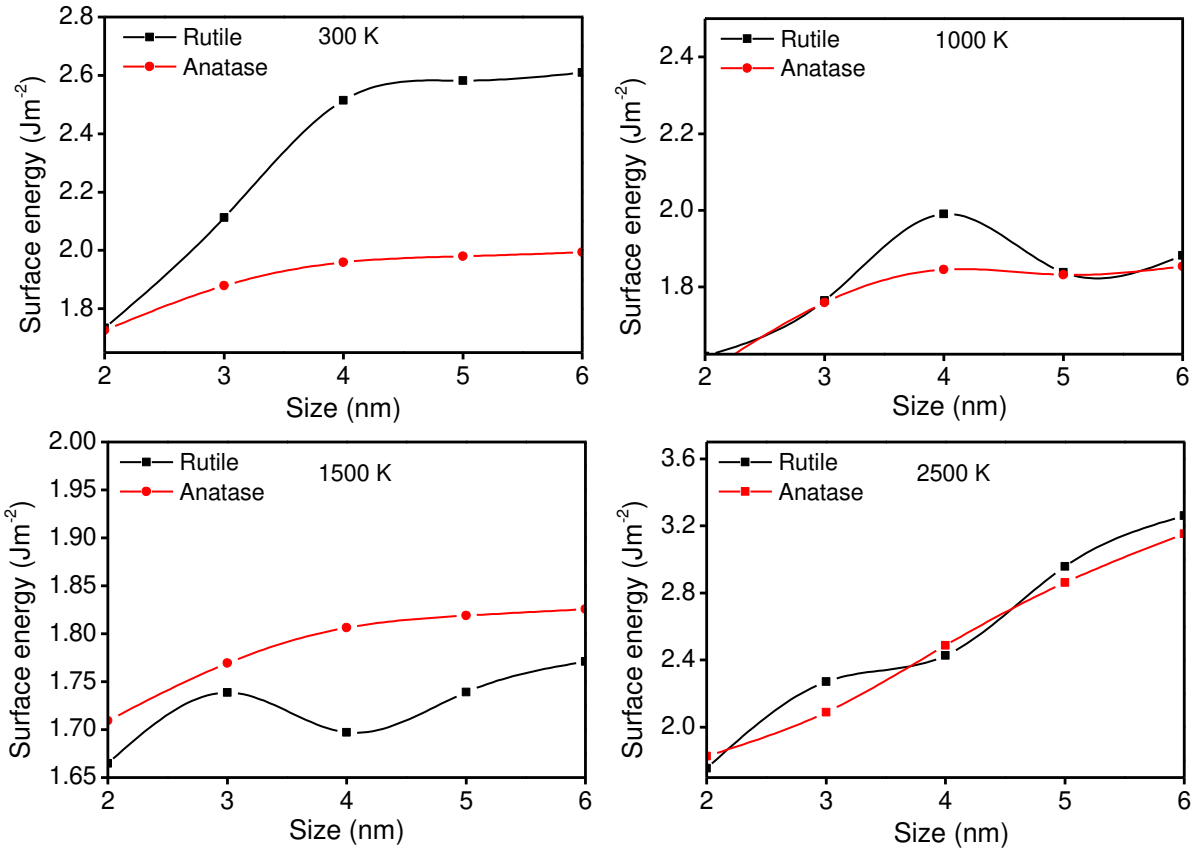

487

488 **Fig. 14** Comparison of surface energy for anatase and rutile nanoparticles at different
489 temperatures as a function of particle size

490 The case of surface energy increasing with temperature especially for relatively small anatase
491 particle sizes is due to the fact that the nanoparticles start to show signs of faceting with a non-
492 spherical shape and become molten as the temperature increases (especially around 2500 K) as
493 seen in Fig. 11. This may further mean that the anatase nanoparticles approach the melting
494 point and become liquid-like. These observations show that the surface energy contribution to
495 thermal properties such as melting point of nanoparticles is significant especially at small
496 particle sizes(Naicker et al., 2005). Furthermore, Fig. 14 shows an increase in surface energy
497 of rutile nanoparticles for increasing particle sizes, for temperatures 300, 1000 and 1500 K. At
498 2500 K, the surface energy of anatase and rutile particles is seen to increase up to a particle
499 size of 6 nm. Overall, observations suggest that surface energy directly controls the shape of
500 TiO_2 nanoparticles at different temperatures.

3.3.3 *Calculation of surface energy of TiO_2 nanoparticles in water under room temperature*

Surface energy of the particles in water under 300K was calculated for different particle sizes ranging from 2–6 nm and phases using the following expression (Okeke et al., 2012);

$$U_{surface} = \frac{U_{TIO_2+H_2O} - \left(nU_{bulk} + U_{H_2O}\right)}{A} \quad (6)$$

Where $U_{TiO2+H2O}$ is the total energy of the nanoparticle and water together, n is the number of TiO_2 molecules, U_{H2O} is the energy of pure water and A is the surface area of the nanoparticle. Results of surface energy for the anatase and rutile nanoparticles in water and vacuum environments are shown in Fig. 15. Surface energy of anatase and rutile nanoparticles in both environments is seen to increase significantly with increase in particle size until 4 nm, above which no significant increase in surface energy is observed. Surface energy of anatase nanoparticles in vacuum is seen to be higher than that in water by about 50% for the smaller particles (i.e. 2 and 3nm) and about 35% for the larger particles (i.e. 4 to 6 nm) (Okeke et al., 2012). These figures for the rutile nanoparticles studied here are about 30% and 20% respectively. Surface energy of rutile nanoparticles is also seen to be lower in water when compared to vacuum environment. Similar to our work, Hummer et al. (2013) also observed higher surface energy for rutile compared to anatase faceted nano particles (of less than 3nm size) under both vacuum and liquid environments. This could be due to water molecules binding strongly to the surface of anatase and rutile nanoparticles, thereby relaxing their surface energy and stabilizing the particles in an aqueous environment (Hummer et al., 2013).

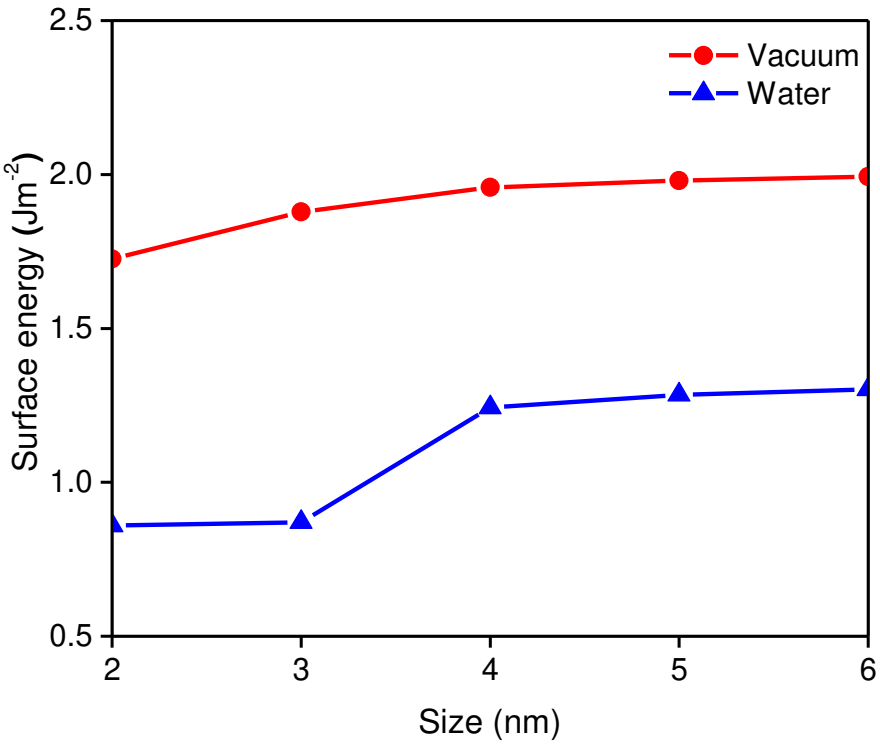

(a)

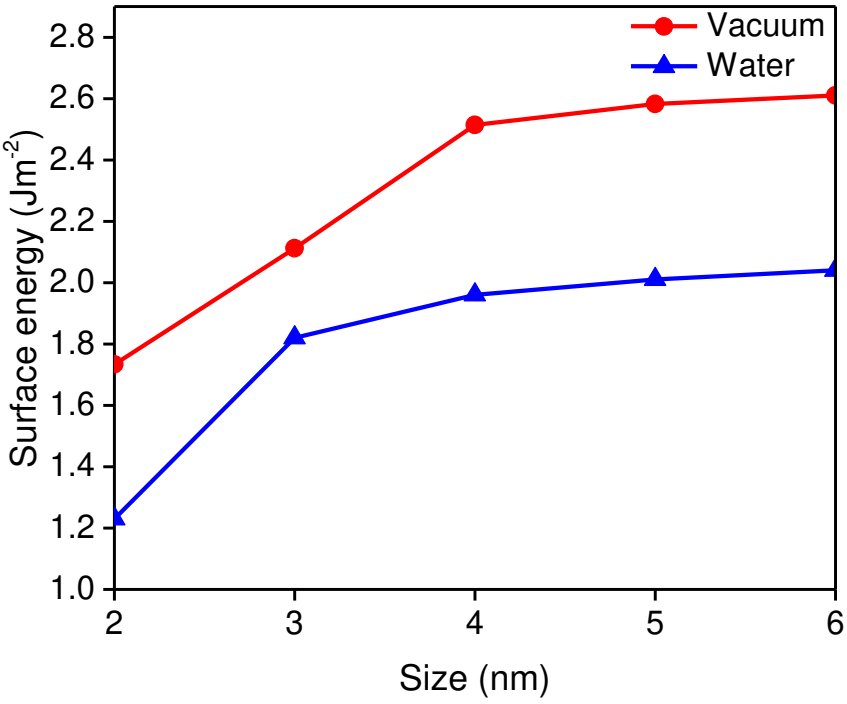

(b)

Fig. 15 Surface energy of (a) anatase and (b) rutile TiO_2 nanoparticles in water and vacuum environments at 300 K

4 Conclusions

MD simulations were performed for the thermodynamic, structural and surface energy of anatase and rutile TiO_2 nanoparticles. The variation of potential energy of the system, with temperature for different nanoparticle sizes, was used to evaluate the melting point of TiO_2 anatase and rutile nanoparticles. It was observed that the temperature associated with the melting transition increased with increasing particle size. Here, the potential energy change associated with the melting transition for anatase was seen to be less than that for rutile nanoparticles, suggesting that for particle sizes considered in this study, rutile is the most thermally stable phase. The RDF trends for both anatase and rutile nanoparticles were linked to the variation of potential energy of the system with temperature. We observed that the change in energy gradient associated with the melting transition occurred at almost similar temperatures associated with the stretching and broadening of the RDF's. The temperature (corresponding to the melting transition) at which the RDF's began to stretch and broaden was observed to be lower for the case of anatase, which suggests that rutile is the more stable phase for nanoparticles within the size range in this study. Further observations on the structural changes in anatase and rutile nanoparticles after MD simulations at different temperatures revealed that non-spherical, rod-like TiO_2 nanoparticles at the nanoscale in rutile phase tends to be thermodynamically more stable. This was also reflected in their respective RDF plots. Results also suggest that surface energy directly controls the shape of TiO_2 nanoparticles at different temperatures. Surface energy of anatase and rutile nanoparticles in water is seen to be lower than that in vacuum. The strong binding of water molecules on the surface atoms of the particles relaxes their surface energy, hence the lower surface energy in water (Hummer et al 2013). In both environments, surface energy of both anatase and rutile nanoparticles is seen to increase to a maximum at about 4 nm, after which no further significant increase is observed.

Furthermore, information provided in this will give more understanding of such fundamental properties for developing new applications, for example in the area of thermal enhancement of nanofluids, which will be presented in future publications. The fundamental properties presented here could further help to study scaling-up production methodologies of TiO_2 nanoparticles using multi-scale methodologies in which such basic properties could form as input to higher level studies.

Nomenclature

$U(r_{ij})$	interaction energy
r_{ij}	distance between sites i and j
q	partial charge
$G(r)$	probability of locating an atom at a distance r from a reference atom compared to a homogenous material of the same number density
$n_{ij}(r)$	coordination number
ΔU_{SE}	surface energy
A	surface area
U_{bulk}	bulk energy
$U_{cluster}$	potential energy of nanoparticle

Greek symbols

ρ	density

References

A. Ahmad, G.H.A., Salman Aziz. 2006. Synthesis and applications of TiO2 nanoparticles. *Pakistan Engineering Congress, 70th Annual Session Proceedings.*

Ahmad, M.I. and Bhattacharya, S.S. 2009. Size effect on the lattice parameters of nanocrystalline anatase. *Applied Physics Letters.* **95**(19), pp.191906-191906-3.

Alimohammadi, M. and Fichthorn, K.A. 2009. Molecular Dynamics Simulation of the Aggregation of Titanium Dioxide Nanocrystals: Preferential Alignment. *Nano Letters.* **9**(12), pp.4198-4203.

Bandura, A.V. and Kubicki, J.D. 2003. Derivation of Force Field Parameters for TiO2−H2O Systems from ab Initio Calculations. *The Journal of Physical Chemistry B.* **107**(40), pp.11072-11081.

Banfield, J.F.Bischoff, B.L. and Anderson, M.A. 1993. TiO2 accessory minerals: coarsening, and transformation kinetics in pure and doped synthetic nanocrystalline materials. *Chemical Geology.* **110**(1–3), pp.211-231.

Brostow, W. 1977. Radial distribution function peaks and coordination numbers in liquids and in amorphous solids. *Chemical Physics Letters.* **49**(2), pp.285-288.

Cai, Q.Buts, A.Seaton, N.A. and Biggs, M.J. 2008. A pore network model for diffusion in nanoporous carbons: Validation by molecular dynamics simulation. *Chemical Engineering Science.* **63**(13), pp.3319-3327.

Chaudhari, G.N.Bambole, D.R.Bodade, A.B. and Padole, P.R. 2006. Characterization of nanosized TiO2 based H2S gas sensor. *Journal of Materials Science.* **41**(15), pp.4860-4864.

Chen, C.-L. and Weng, H.-S. 2005. Nanosized CeO2-supported metal oxide catalysts for catalytic reduction of SO2 with CO as a reducing agent. *Applied Catalysis B: Environmental.* **55**(2), pp.115-122.

Collins, D.R.Smith, W.Harrison, N.M. and Forester, T.R. 1996. Molecular dynamics study of TiO2 microclusters. *Journal of Materials Chemistry.* **6**(8), pp.1385-1390.

Connolly, M. 1983. Analytical molecular surface calculation. *Journal of Applied Crystallography.* **16**(5), pp.548-558.

Filyukov, D.Brodskaya, E.Piotrovskaya, E. and de Leeuw, S. 2007. Molecular-dynamics simulation of nanoclusters of crystal modifications of titanium dioxide. *Russian Journal of General Chemistry.* **77**(1), pp.10-16.

595 Gale, J. and Rohl, A. 2003. The general utility lattice program (GULP).
596 Haverkamp, R.G. 2010. A Decade of Nanoparticle Research in Australia and New Zealand.
597 *Particulate Science and Technology: An International Journal.* **28**(1), pp.1 - 40.
598 Hines, A.Walls, H. and Jethani, K. 1985. Determination of the coordination number of liquid
599 metals near the melting point. *Metallurgical Transactions A.* **16**(1), pp.267-274.
600 Hoang, V.V. 2008. The glass transition and thermodynamics of liquid and amorphous TiO 2
601 nanoparticles. *Nanotechnology.* **19**(10), p105706.
602 Horn, M.Schwerdtfeger, C. and Meagher, E. 1972. Refinement of the structure of anatase at
603 several temperatures. *Zeitschrift für Kristallographie.* **136**(3-4), p273.
604 Hu, J.Q.Ma, X.L.Shang, N.G.Xie, Z.Y.Wong, N.B.Lee, C.S. and Lee, S.T. 2002. Large-Scale
605 Rapid Oxidation Synthesis of SnO2 Nanoribbons. *The Journal of Physical Chemistry*
606 *B.* **106**(15), pp.3823-3826.
607 Hummer, D.R.Kubicki, J.D.Kent, P.R.C. and Heaney, P.J. 2013. Single-Site and Monolayer
608 Surface Hydration Energy of Anatase and Rutile Nanoparticles Using Density
609 Functional Theory. *The Journal of Physical Chemistry C.* **117**(49), pp.26084-26090.
610 Hummer, D.R.Kubicki, J.D.Kent, P.R.C.Post, J.E. and Heaney, P.J. 2009. Origin of
611 Nanoscale Phase Stability Reversals in Titanium Oxide Polymorphs. *The Journal of*
612 *Physical Chemistry C.* **113**(11), pp.4240-4245.
613 Isaak, D.G.Carnes, J.D.Anderson, O.L.Cynn, H. and Hake, E. 1998. Elasticity of TiO2 rutile
614 to 1800 K. *Physics and Chemistry of Minerals.* **26**(1), pp.31-43.
615 Jagtap, N.Bhagwat, M.Awati, P. and Ramaswamy, V. 2005. Characterization of
616 nanocrystalline anatase titania: an in situ HTXRD study. *Thermochimica Acta.* **427**(1-
617 2), pp.37-41.
618 Kermanpur, A.Ghassemali, E. and Salemizadeh, S. 2008. Synthesis and characterisation of
619 microporous titania membranes by dip-coating of anodised alumina substrates using
620 sol–gel method. *Journal of Alloys and Compounds.* **461**(1–2), pp.331-335.
621 Kirk, R.E.Othmer, D.F.Kroschwitz, J.I. and Howe-Grant, M. 1998. *Encyclopedia of chemical*
622 *technology.* John Wiley & Sons.
623 Koparde, V.N. and Cummings, P.T. 2005. Molecular Dynamics Simulation of Titanium
624 Dioxide Nanoparticle Sintering. *The Journal of Physical Chemistry B.* **109**(51),
625 pp.24280-24287.
626 Koparde, V.N. and Cummings, P.T. 2007. Molecular Dynamics Study of Water Adsorption
627 on TiO2 Nanoparticles. *The Journal of Physical Chemistry C.* **111**(19), pp.6920-6926.

628 Koparde, V.N. and Cummings, P.T. 2008. Phase Transformations during Sintering of Titania
629 Nanoparticles. *ACS Nano.* **2**(8), pp.1620-1624.
630 Lazzeri, M.Vittadini, A. and Selloni, A. 2001. Structure and energetics of stoichiometric
631 ${\mathrm{TiO}}_{2}$ anatase surfaces. *Physical Review B.* **63**(15), p155409.
632 Lihitkar, N.B.Abyaneh, M.K.Samuel, V.Pasricha, R.Gosavi, S.W. and Kulkarni, S.K. 2007.
633 Titania nanoparticles synthesis in mesoporous molecular sieve MCM-41. *Journal of*
634 *Colloid and Interface Science.* **314**(1), pp.310-316.
635 Mark, P. and Nilsson, L. 2001. Structure and Dynamics of the TIP3P, SPC, and SPC/E Water
636 Models at 298 K. *The Journal of Physical Chemistry A.* **105**(43), pp.9954-9960.
637 *Materials Studio suite of crystallographic programs.* [Online]. Available from:
638 http://www.accelrys.com/.
639 Matsui, M. and Akaogi, M. 1991. Molecular Dynamics Simulation of the Structural and
640 Physical Properties of the Four Polymorphs of TiO2. *Molecular Simulation.* **6**(4-6),
641 pp.239-244.
642 Mishra, S.Jha, P. and Pratap, A. 2012. Study of size-dependent glass transition and
643 Kauzmann temperature of titanium dioxide nanoparticles. *Journal of Thermal*
644 *Analysis and Calorimetry.* **107**(1), pp.65-68.
645 Naicker, P.K.Cummings, P.T.Zhang, H. and Banfield, J.F. 2005. Characterization of
646 Titanium Dioxide Nanoparticles Using Molecular Dynamics Simulations. *The*
647 *Journal of Physical Chemistry B.* **109**(32), pp.15243-15249.
648 Oh, S.W.Park, S.-H. and Sun, Y.-K. 2006. Hydrothermal synthesis of nano-sized anatase
649 TiO2 powders for lithium secondary anode materials. *Journal of Power Sources.*
650 **161**(2), pp.1314-1318.
651 Okeke, G.Hammond, R. and Antony, S.J. 2012. Analysis of Structural and Surface Properties
652 of TiO2 Nanoparticles in Water and Vacuum Using Molecular Dynamics Modeling
653 and Simulations. *Journal of Nanofluids.* **1**(1), pp.21-27.
654 Okeke, G.Hammond, R. and Joseph Antony, S. 2013a. Influence of size and temperature on
655 the phase stability and thermophysical properties of anatase TiO2 nanoparticles:
656 molecular dynamics simulation. *Journal of Nanoparticle Research.* **15**(4), pp.1-9.
657 Okeke, G.Hammond, R.B. and Antony, S.J. 2013b. Molecular Dynamics Simulation of
658 Anatase TiO2 Nanoparticles. *Journal of Nanoscience and Nanotechnology.* **13**(2),
659 pp.1047-1052.

660 Okeke, G.Witharana, S.Antony, S. and Ding, Y. 2011. Computational analysis of factors
661 influencing thermal conductivity of nanofluids. *Journal of Nanoparticle Research.*
662 **13**(12), pp.6365-6375.
663 Oliver, P.M.Watson, G.W.Toby Kelsey, E. and Parker, S.C. 1997. Atomistic simulation of
664 the surface structure of the TiO2 polymorphs rutileand anatase. *Journal of Materials*
665 *Chemistry.* **7**(3), pp.563-568.
666 Onozuka, K.Ding, B.Tsuge, Y.Naka, T.Yamazaki, M.Sugi, S.Ohno, S.Yoshikawa, M. and
667 Shiratori, S. 2006. Electrospinning processed nanofibrous TiO 2 membranes for
668 photovoltaic applications. *Nanotechnology.* **17**(4), p1026.
669 Park, S.-J.Kang, Y.C.Evans, E.A. and Ramsier, R.D. 2010. Physical Characteristics of Titania
670 Nanofibers Synthesized by Sol-Gel and Electrospinning Techniques. *Journal of*
671 *Engineered Fibers and Fabrics.*
672 Pradhan, S.K.Reucroft, P.J.Yang, F. and Dozier, A. 2003. Growth of TiO2 nanorods by
673 metalorganic chemical vapor deposition. *Journal of Crystal Growth.* **256**(1–2), pp.83-
674 88.
675 Reyes-Coronado, D.Rodríguez-Gattorno, G.Espinosa-Pesqueira, M.E.Cab, C.Coss, R.d. and
676 Oskam, G. 2008. Phase-pure TiO 2 nanoparticles: anatase, brookite and rutile.
677 *Nanotechnology.* **19**(14), p145605.
678 Ribeiro, C.Vila, C.Milton Elias de Matos, J.Bettini, J.Longo, E. and Leite, E.R. 2007. Role of
679 the Oriented Attachment Mechanism in the Phase Transformation of Oxide
680 Nanocrystals. *Chemistry – A European Journal.* **13**(20), pp.5798-5803.
681 Sheng, Z.Hu, Y.Xue, J.Wang, X. and Liao, W. 2012. A novel co-precipitation method for
682 preparation of Mn–Ce/TiO2 composites for NOx reduction with NH3 at low
683 temperature. *Environmental Technology.* **33**(21), pp.2421-2428.
684 Skripov, V.P.Koverda, V.P. and Skokov, V.N. 1981. Size effect on melting of small particles.
685 *physica status solidi (a).* **66**(1), pp.109-118.
686 Smith, W.Forester, T.R. and Todorov, I.T. 2010. The DL_POLY_2 User Manual. *STFC*
687 *Daresbury Laboratory.* **Version 2.21**.
688 Song, D.-P.Liang, Y.-C.Chen, M.-J. and Bai, Q.-S. 2009. Molecular dynamics study on
689 surface structure and surface energy of rutile TiO2 (1 1 0). *Applied Surface Science.*
690 **255**(11), pp.5702-5708.
691 Soo-Jin Park, Y.C.K., Ju Y. Park, Ed A. Evans, Rex D. Ramsier, and George G. Chase. 2010.
692 Physical Characteristics of Titania Nanofibers Synthesized by Sol-Gel and

693 Electrospinning Techniques. *Journal of Engineered Fibers and Fabrics.* **5**(1), pp.50-
694 56.
695 Sugiyama, K. and Takéuchi, Y. 1991. *The crystal structure of rutile as a function of*
696 *temperature up to 1600°C*. Zeitschrift für Kristallographie. 194. p.305. [Accessed
697 2014-07-02t14:40:58.733+02:00]. Available from:
698 http://www.degruyter.com/view/j/zkri.1991.194.issue-3-4/zkri.1991.194.3-
699 4.305/zkri.1991.194.3-4.305.xml.
700 Takagi, M. 1954. Electron-Diffraction Study of Liquid-Solid Transition of Thin Metal Films.
701 *Journal of the Physical Society of Japan.* **9**(3), pp.359-363.
702 Tang, H.Berger, H.Schmid, P.E.Lévy, F. and Burri, G. 1993. Photoluminescence in TiO2
703 anatase single crystals. *Solid State Communications.* **87**(9), pp.847-850.
704 Wronski, C.R.M. 1967. The size dependence of the melting point of small particles of tin.
705 *British Journal of Applied Physics.* **18**(12), p1731.
706 Xia, Y.Yang, P.Sun, Y.Wu, Y.Mayers, B.Gates, B.Yin, Y.Kim, F. and Yan, H. 2003. One-
707 Dimensional Nanostructures: Synthesis, Characterization, and Applications.
708 *Advanced Materials.* **15**(5), pp.353-389.
709 Yang, J.Mei, S. and Ferreira, J.M.F. 2001. Hydrothermal Synthesis of Nanosized Titania
710 Powders: Influence of Tetraalkyl Ammonium Hydroxides on Particle Characteristics.
711 *Journal of the American Ceramic Society.* **84**(8), pp.1696-1702.
712 Zhang, H. and Banfield, J.F. 2000. Understanding Polymorphic Phase Transformation
713 Behavior during Growth of Nanocrystalline Aggregates: Insights from TiO2. *The*
714 *Journal of Physical Chemistry B.* **104**(15), pp.3481-3487.
715 Zhang, H.Chen, B.Banfield, J.F. and Waychunas, G.A. 2008. Atomic structure of nanometer-
716 sized amorphous TiO_{2}. *Physical Review B.* **78**(21), p214106.
717 Zhang, H. and F. Banfield, J. 1998. Thermodynamic analysis of phase stability of
718 nanocrystalline titania. *Journal of Materials Chemistry.* **8**(9), pp.2073-2076.
719 Zheng, L.Xu, M. and Xu, T. 2000. TiO2−x thin films as oxygen sensor. *Sensors and*
720 *Actuators B: Chemical.* **66**(1–3), pp.28-30.

721